

A STEP TOWARDS THE CHARACTERISATION OF SAR MODE ALTIMETRY DATA OVER INLAND WATERS - SHAPE PROJECT

Pierre Fabry⁽¹⁾, Nicolas Bercher⁽¹⁾, Américo Ambrósio ⁽²⁾, Marco Restano ⁽³⁾ and Jérôme Benveniste ⁽⁴⁾

⁽¹⁾ ALONG-TRACK S.A.S., 43B rue de Bertheaume, 29217, Plougonvelin, France, contact@along-track.com

⁽²⁾ Deimos/ESRIN, via Galileo Galilei, Frascati, 00044, Italy

⁽³⁾ Serco/ESRIN, via Galileo Galilei, Frascati, 00044, Italy

⁽⁴⁾ ESA-ESRIN, via Galileo Galilei, Frascati, 00044, Italy

ABSTRACT

Inland water scenes are highly variable, both in space and time, which leads to a much broader range of radar signatures than ocean surfaces. This applies to both LRM and “SAR” mode (SARM) altimetry. Nevertheless the enhanced along-track resolution of SARM altimeters should help improve the accuracy and precision of inland water height measurements from satellite. The SHAPE project – Sentinel-3 Hydrologic Altimetry Processor prototype – which is funded by ESA through the Scientific Exploitation of Operational Missions Programme Element (contract number 4000115205/15/I-BG) aims at preparing for the exploitation of Sentinel-3 data over the inland water domain. In order to define refine the L1B processor and the retracers for alti-hydrology applications, we need to characterise the SARM Individual Echoes, Multi-Look Stacks as well as 20Hz waveforms over the inland water domain.

This paper deals with the continuation of works presented in 2015 [Fabry et Bercher, Venice 2015b] [Fabry et Bercher, Frascati 2015a/c] where we introduced an automated technique to assess the water fraction within the Beam-Doppler limited footprint through its intersection area with a water mask. We hereby refine the utilisation of these water classes and run the classification on a wider dataset so as to improve the readout of the Range Integrated Power¹ (RIP) parameters and the waveforms versus the Water Fraction.

1. CONTEXT

When a radar altimeter overflies the inland water domain its ground projected footprints often cover many targets that exhibit quite different backscattering properties. The footprints may cover the borders of the water bodies, some islands and/or vegetation in addition to the water bodies themselves. In comparison to the ocean domain, this results into the “land contamination” of the altimeter signals (stacks and waveforms). In some cases man made infrastructure such as bridges, dams, roads and buildings can also be part of the scene that is remotely sensed. Detecting such signatures and filtering them out will result in significant improvements of alti-

¹ RIP. is a 1D signal resulting from the range-wise summation of the 2D Multi-Look Stack (1 stack per record), while the sum in the along-track direction provides the 20Hz SAR waveform.

hydro products (precision improvement). This approach is relevant for both geodetic and repeat orbit altimetry since inland water scenes do change over time (rivers and lakes bathymetry as well as their contours, islands and vegetation do change over seasons). Moreover the precision of the repeat orbit track location is often within a 1km wide corridor along the theoretical ground track. Moreover, the backscattering properties of water bodies depend upon wind stress conditions, surface current and trophic phenomena. The land contamination at nadir may also be complemented with multiple off-nadir water contributions that strongly modify the resulting stacks and waveforms. These also are interesting signatures to be detected.

In this context, altimeters signals cannot be characterised without a better knowledge on the scene under the actual track and footprint location. For this exercise, the use of frequently updated water masks seems unavoidable. To ease the task, a new framework has been set up so as to exploit water masks in an automated manner. The framework is briefly described in section 2. We then apply it to CryoSat-2 data [ESA, 2013] in section 3, for now still with the old static SWBD water mask (Shuttle Radar Topography Mission Water Body Delineation masks) [NGA-USGS, 2003]. Results are analysed in section 4 and preliminary conclusions are drawn in section 5. The many areas of improvement and perspectives are listed in section 6.

2. AUTOMATED FRAMEWORK FOR THE CHARACTERISATION EXERCISE

In order to ease and automate the characterisation exercise, we had to find a simple criteria for the classification of altimeter records. We decided to classify the Level-1 SARM altimetry data from the automated computation of the water fraction within the instrument footprint based on the superimposition of a water mask on the altimeter footprint on ground. This new framework enables us to use water masks derived from radar imaging missions such as Sentinel-1 (and ENVISAT during its overlap period with CryoSat-2). Even though C band radar sensors are at a lower resolution than optical sensors, they ensure a regular update of water masks thanks to their all-weather, night and day imaging capabilities. ALONG-TRACK has its own tool to produce time dependent water masks from Sentinel-1 imagery [Fabry et al. 2015a].

2.1. Principles

Beam-Doppler limited footprints are computed, at each record, from the longitude, latitude, tracker range, satellite altitude and velocity found in CryoSat-2 L1B files and system parameters (3dB antenna beam-width, burst PRF). As depicted in Figure 1, the Beam-Doppler limited footprints are superimposed on water masks in the local Earth-tangential plane (ENU: East North-Up). This makes it possible to compute, for each footprint, the footprint area (FA) as well as the water area (WA) at the intersection with the water masks. We then define the **water fraction** as :

$$WFR = WA / FA. \quad (\text{Eq.1})$$

2.2. Details of the Footprints generation

The along-track or Doppler limited footprint size is related to the satellite velocity V_{sat} , its range to ground h , the central wavelength λ , and the burst PRF :

$$\Delta x = h \cdot \frac{\lambda}{2V_{sat}} \cdot \frac{PRF}{64} \quad (\text{Eq. 2})$$

An approximation of the across-track beam size D is:

$$D = h \cdot \tan\left(\theta_B + \frac{v}{2}\right) - h \cdot \tan\left(\theta_B - \frac{v}{2}\right) \quad (\text{Eq. 3})$$

where,

- θ_B is the 3dB across-track antenna aperture (1.2 deg),

- v is the boresight angle w.r.t. nadir (0 deg here but it can be computed from the attitude angles).

Both Δx and D are computed at each record location with updated parameters.

2.3. Signal properties to be analysed

The objective is to look at specific properties of altimetric signals versus the WFR. The beam behaviour parameters found in the L1B products qualify the Gaussian fit of the Range Integrated Power (RIP). The beam behaviour parameters are the :

- Mean Centre of the Gaussian fit of the RIP,
- Stack Standard Deviation of the Gaussian PDF fitting the RIP : 2nd order moment related to the softness,
- Stack Skewness : asymmetry of the RIP,
- Stack Kurtosis : RIP peakiness (4th order),
- Stack Scaled : the stack amplitude is scaled to capture the dynamics of the received power with a fixed number of bits.

These five parameters have values in the range 0 to 65535 (CryoSat-2 Product Handbook). They should be understood as beam numbers after a division by 100. Moreover, waveforms and parameters in “scaled amplitude” can be converted to a power in Watt :

$$\text{Power[W]} = \text{scaledvalue} * \text{scalefactor} * 10^{-9} * 2^{\text{scalepower}} \quad (\text{Eq.4})$$

3. EXPERIMENTAL SET UP

The experiment presented here relies on 280 CryoSat-2 Baseline-C L1B SARM products over the downstream Manaus section of the Amazon river for the whole year 2014.

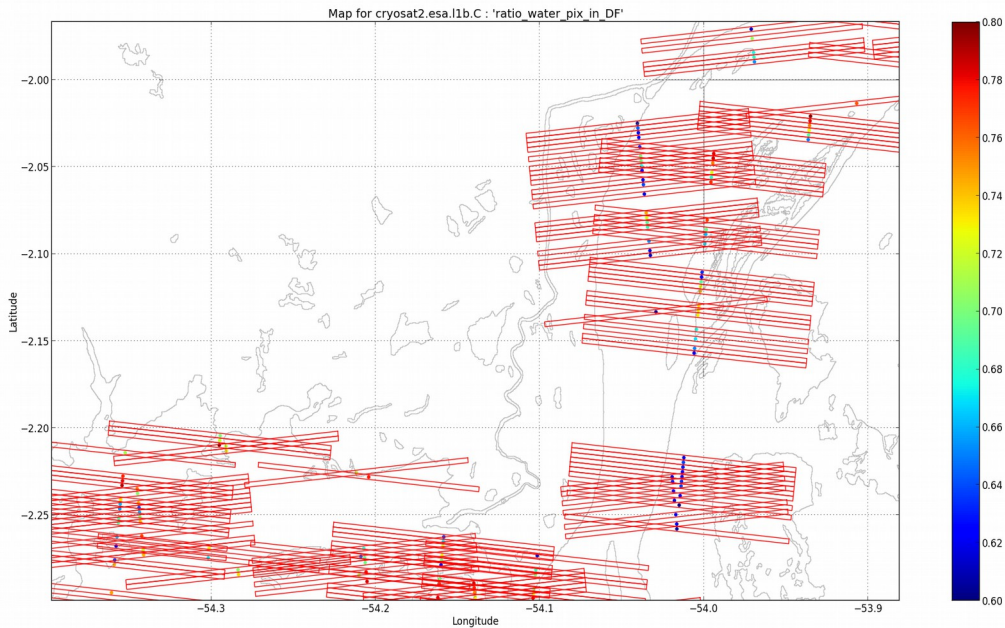


Figure 1: CryoSat-2 Baseline-C Beam-Doppler limited footprints (20Hz records) over downstream Amazon together with SWBD water masks and a central dot whose color indicates the water fraction (60-80%) in each footprint.

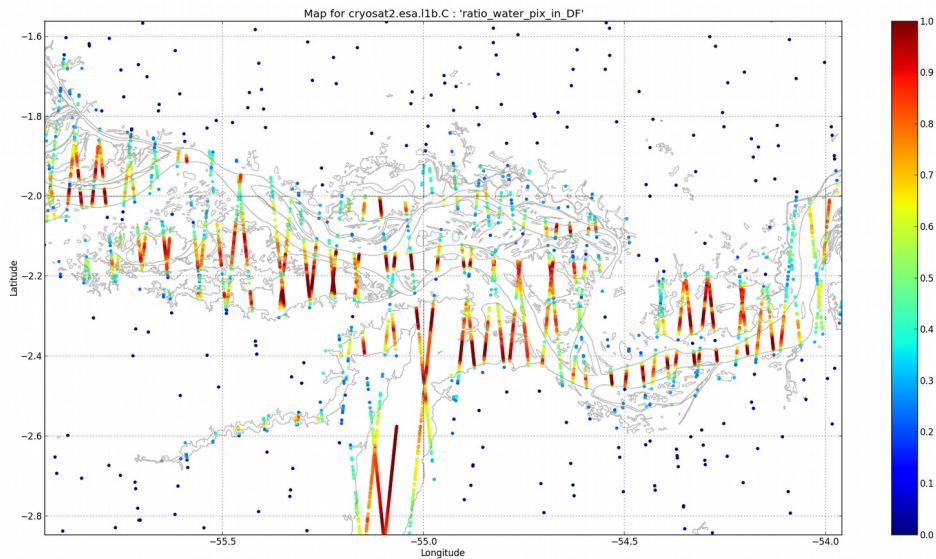


Figure 2: Records with their color coded Water Fraction. Zoom on a part of the downstream Amazon river represented by its SWBD water mask.

Any record whose footprint intersects more than 1 SWBD tile is rejected. This is a negligible loss and 319523 records are successfully extracted. They populate an unbalanced histogram composed of 5 WFR classes of equal size. The population of each class is then balanced through the random selection of about 3200 individuals per class (the smallest class population). The waveforms and RIP parameters of these classes are then compared. Figure 2 is a zoom on a part of the downstream Amazon river, represented by the SWBD water mask in grey, having superimposed the balanced population of color coded records where the colormap represents the WFR.

4. RESULTS

In the following, results are provided with a stable color code for the 5 WFR classes : class 1 : dark blue for [0-20]%, class 2 : green for [20-40]%, class 3 : red for [40-60]%, class 4 : cyan for [60-80]% and class 5 : magenta for [80-100]%.

The mean echo power waveforms (in Watt) of the 5 classes are shown in Figure 3. They result from about 3200 waveforms for each class. Except for the highest WFR class (magenta), they are quite different from ocean waveforms.

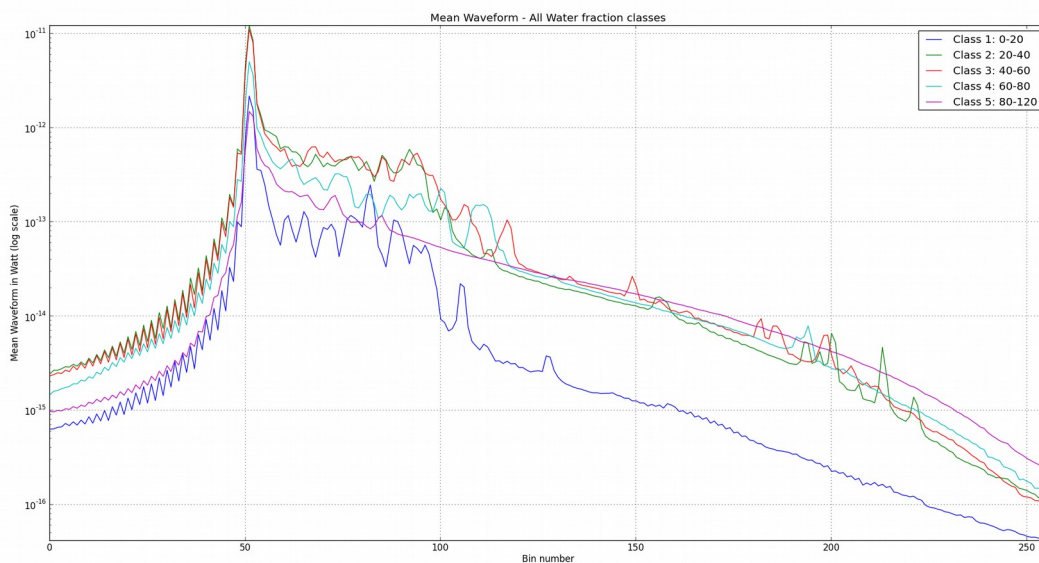


Figure 3: CryoSat-2 SAR Mode Baseline-C mean power waveforms in Watt for the 5 Water Fraction Classes. Ordinates axis in log10 scale.

Oscillations and multiple peaks are found in the mean waveforms, except at the highest WFR class (magenta). This comes from numerous multi-peaks waveforms or from a variable position of the main peak. This is depicted in Figure 4 for the lowest WFR class where axes are in linear scales. Such a variety of waveforms comes from the fact that water is not always at nadir while the location of the peaks depends on the across track position of the waterbodies (left and/or right of the ground track).

Indeed, in the low WFR cases, water bodies are diversely spread over the footprint, going from “most of the water area is at nadir” to “most of the water area is at far end” of the footprint. The backscattering diagram of surface water depends on water roughness which in turn relies on wind fetch and surface current, as well as on the incidence angle of electromagnetic waves coming from the radar. Both the antenna and targets backscattering diagrams combine into a wide variety of Stacks and RIPs.

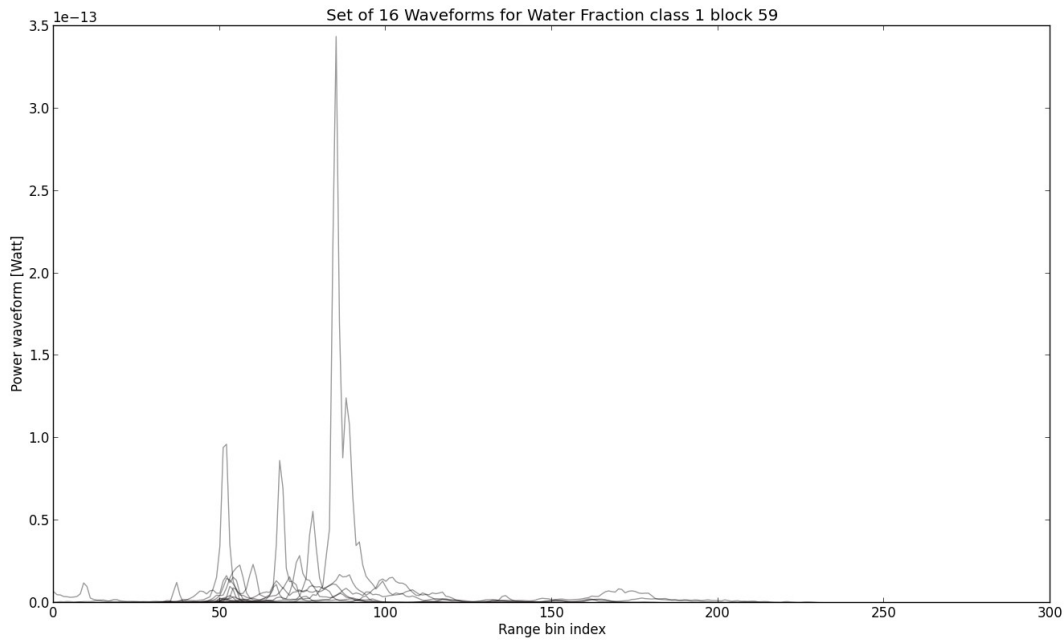


Figure 4: Set of CryoSat-2 Baseline-C L1B power waveforms in Watt for Water Fraction class 1 over Manaus downstream Amazon in 2014.

Figure 5 shows that the scaled amplitude of the RIP in classes with a WFR above 60% is better focused around the mean value than classes with low WFR. Indeed, water surfaces do scatter a more stable portion of the power back to the instrument (specular backscattering).

In Figure 6, the Standard Deviation of the RIP indicates how the incident radar power is backscattered from the footprint into many azimuth look angles (Doppler Beams). The highest WFR classes (4 and 5) experience a higher mean Standard Deviation of the RIP than other classes. As these classes encompass large cross sections of the river, the smooth variation in their angular power distribution in the RIP could be related to both wind fetch and the capture of river regime changes (higher roughness resulting in a diffuse scattering). On the other hand, footprints with a very small water content statistically have a small RIP Standard Deviation which means that the along-track angular power distribution varies faster around the stack centre. The most likely explanation is that small water bodies are smooth specular surfaces in most cases (reduced impact of wind stress). Figure 6 also shows that the lowest WFR class is quite heterogeneous.

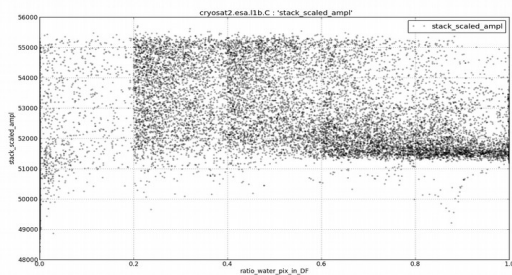


Figure 5: Scaled amplitude of the RIP versus Water Fraction in CryoSat-2 Baseline-C L1B Beam-Doppler footprints over the Downstream Manaus section of the Amazon river. About 16000 records are displayed here to cover the 5 Water Fraction classes (3200 individuals per class).

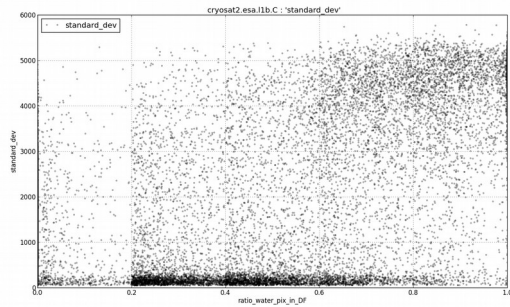


Figure 6: Standard Deviation of the Gaussian PDF fitting the RIP versus Water Fraction in CryoSat-2 Baseline-C L1B Beam-Doppler footprints over the Downstream Manaus section of the Amazon river. About 16000 records are displayed here to cover the 5 Water Fraction classes (3200 individuals per class).

In complement, the Kurtosis of the RIP, displayed in figure 7, confirms and enhances results obtained with the Standard Deviation; footprints with WFR greater than 80% have an angular power distribution that varies smoothly in azimuth around the central beam. The Kurtosis of the RIP at high WFR values is well focused around its mean value that is close to zero. For intermediate WFR classes, the Kurtosis spreads over a wider range of values and the mean Kurtosis is higher. This is in line with the observation made on the Standard Deviation where a relatively peaky angular response was found on WFR from 20% to 60%. The lowest WFR scenarios are more difficult to analyse.

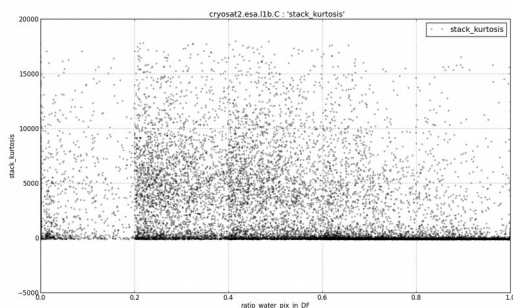


Figure 7: Kurtosis of the RIP versus Water Fraction in CryoSat-2 Baseline-C L1B Beam-Doppler footprints over the Downstream Manaus section of the Amazon river. About 16000 records are displayed here to cover the 5 Water Fraction classes (3200 individuals per class).

The Skewness of the RIP in figure 8 reinforces the previous interpretations of both the Standard Deviation and the Kurtosis of the RIP. The highest WFR classes (4 and 5) statistically exhibit small Skewness values (close to zero). This means that the Stack is quite symmetrical, in the along-track dimension. This is coherent with the fact that these records cover large water areas at the central burst, which lowers the impact of side-lobe effects and off-nadir glares that could otherwise

unbalance the stack from the side lobes of the fore and aft bursts. Intermediate WFR classes (2 and 3) show much more spread values of the RIP Skewness with a much higher mean value showing that the Stack is often not symmetrical in the azimuth dimension around its central beam. This may come from side-lobe effects and off-nadir glare of some beams at the fore and/or aft part of the Stack at these intermediate classes. The lowest WFR class remains difficult to analyse due to its huge diversity.

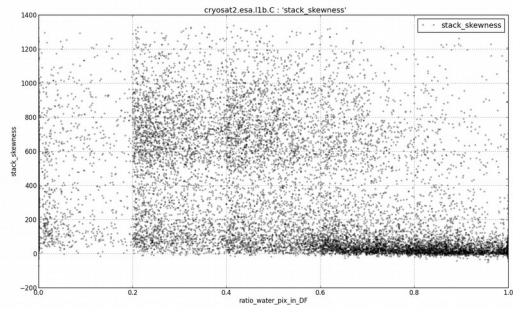


Figure 8: Skewness of the RIP versus the Water Fraction found in CryoSat-2 Baseline-C L1B Beam-Doppler footprints over the Downstream Manaus section of the Amazon river. About 16000 records are displayed here to cover the 5 Water Fraction classes (3200 individuals per class).

The huge diversity within the 1st WFR class (dark blue) can be confirmed by the plot of the Skewness of the RIP versus the Scaled Amplitude and the WFR in Figure 9. This translates into a higher dispersion of both the Scaled Amplitudes and Skewness of the RIP but this is also true for the centre of the RIP in Figure 10. These characteristics could indicate a strong influence of side lobe effects and off-nadir glares from water bodies seen at fore and aft bursts.

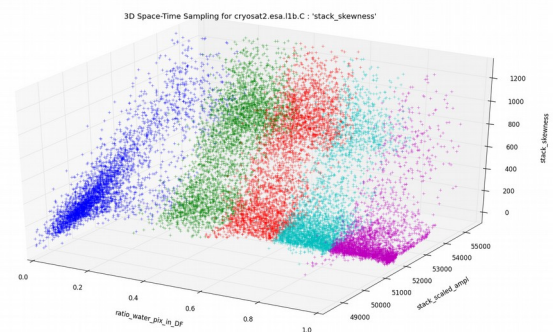


Figure 9: Skewness of the RIP versus Scaled Amplitude and the WFR in CryoSat-2 Baseline-C L1B Beam-Doppler footprints over the Downstream Manaus section of the Amazon river. About 16000 records are displayed here to cover the 5 Water Fraction classes (3200 individuals per class).

Figure 10 actually provides the Centre of the RIP versus the Kurtosis of the RIP and the WFR. The low WFR class (dark blue) exhibits a high dispersion of the beam number at the centre of the fitted Gaussian function and a small dispersion of RIP Kurtosis. This confirms the

high diversity of backscattering phenomena in this class, unless very different Stack sizes have been used over non water records.

The high WFR class (magenta) exhibits a small dispersion of the beam number at the centre of the fitted Gaussian function and a small dispersion of RIP Kurtosis. This class experiences a dominant backscattering mechanism with a slight dispersion to account for the various water roughness cases. There is high probability for water at nadir and reduced side lobe impact leading to homogeneous features of the class. The intermediate classes experience a dispersion in terms of RIP peakiness but maintain a stable position of their Stack centre.

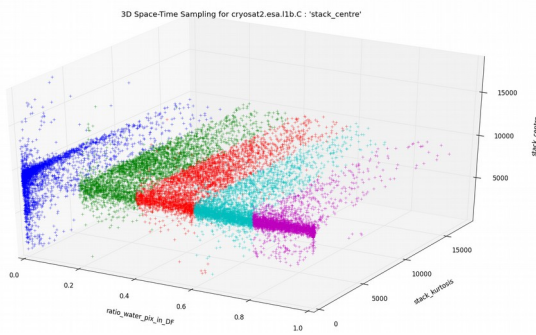


Figure 10: Centre of the RIP versus Kurtosis of the RIP and Water Fraction in CryoSat-2 Baseline-C L1B Beam-Doppler footprints over the Downstream Manaus section of the Amazon river. About 16000 records are displayed here to cover the 5 Water Fraction classes (3200 individuals per class).

In practice the actual power of many looks (and therefore the shape of the RIP) is impacted by several contributions :

- the water fraction (WFR),
- the distribution of water bodies across the Doppler Footprint,
- the along-track (or burst to burst) evolution of the WFR combined to the antenna side lobes. The looks for which a side lobe is directed to a water area will have a ghost contribution to the RIP, thus modifying the shape of the RIP and the Gaussian fit,
- the contribution of small water surfaces not accounted for in SWBD water masks.

5. CONCLUSIONS

The characteristics that have been found in altimeter signals over inland waters in the Amazon basin are here summarized. Still, we invite the reader to be cautious with these preliminary conclusions since errors have recently been reported in baseline-C products and we do not know if they affect only L2 products or also the L1B data used here. Moreover, the adopted water masks is very old (2003) and probably not exhaustive enough regarding the smaller water surfaces [NGA-USGS, 2003]. The low WFR classes from these water masks

may have changed. Still, the following characteristics should remain valid:

- footprints with a WFR above 60% experience a relatively stable backscattering mechanism e.g. a more stable portion of the received power is backscattered to the radar altimeter (specular backscattering).
- while the WFR decreases from 60% to 0%, a broader range of backscattering mechanisms is involved and this translates into an extended range of scaled amplitudes at the RIP.

The analysis of the Kurtosis and Standard Deviation of the RIP indicates that :

- footprints with a WFR above 60% (encompassing many large cross sections of the river), experience smooth variations of the angular power distribution, in the along-track dimension. This could be related both to wind fetch and to the capture of river regime changes (higher roughness).
- on the other hand, the angular power distribution of footprints with a WFR within 20% to 60% is more peaky in many cases. The explanation could be that small water bodies are smooth specular surfaces in most cases (reduced impact of wind stress).

The analysis of Skewness of the RIP indicates that :

- records with a WFR above 60% have a quite symmetrical angular power distribution in the along-track dimension. This is coherent with the fact that these records cover large water areas at the central burst, which lowers the impact of side-lobe effects and off-nadir glares at fore and aft bursts, that could otherwise unbalance the stack.
- records with a WFR within 20% to 60% often do not have a symmetrical Stack in the azimuth dimension. This may come from side-lobe effects and from off-nadir glares of some beams in fore and/or aft parts of the Stack. In depth analysis of these cases is required.

- From many aspects (peakiness, asymmetry, scaled amplitude, stack centre ...) records with a WFR below 20% are difficult to characterise. This may be due to a higher diversity of the involved backscattering mechanisms and possibly to a higher sensitivity to side-lobe effects and off-nadir glares. This is to be further analysed as it requires the information on the number of beams that have been used to build the Stacks (this number is available in Baseline-C products). Records with no water (assuming that the static water mask is still valid and remains valid in all seasons) may also

have specific characteristics that should not be mixed with the case of footprints with a non 0% WFR.

- The high WFR class (**magenta**) exhibits a small dispersion of the beam number at the centre of the fitted Gaussian function and a small dispersion of RIP Kurtosis. This class experiences a dominant backscattering mechanism with a slight dispersion to account for the various water roughness cases. There is high probability for water at nadir and reduced side lobes impact leading to homogeneous features of the class.

- The intermediate classes experience a dispersion in terms of RIP peakiness but maintain a stable position of their Stack centre.

These results apply to Amazon basin and there is no evidence yet that they also apply to other basins. These new and interesting results are pushing us to go further in this direction. The readout of our experiment could be improved in many aspects as described in the last section.

6. ONGOING WORK AND PERSPECTIVES

The following evolutions of our experiment are needed and most of them are already being implemented :

- repeat the exercise over the year 2015 and compare with the results obtained for 2014.
- rerun the experiment on baseline B to assess the potential regressions of baseline-C (jumps found in Baseline-C L1B could be related to changes in the platform attitude processing).
- introduce the 0% and the 100% WFR classes.
- apply the Scaled Amplitude to Watt conversion to the RIP. check all units and apply the correct dividers: for example, the Stack Centre should be divided by 100 in baseline C. The plot should mention "beam numbers" as units.
- refine the analysis of pathological cases by plotting footprints in the colour of the corresponding water fraction class (5 colours) with a dot inside corresponding to the exact water fraction value.
- compute the Antenna Pattern weighted WFR instead of the raw WFR.
- provide outputs of our waveform analysis tool, to help analysing the diversity of Waveforms. The tool plots in one window the Range Chronograms of Waveforms in Watt (RCG) with water masks in background, and, in a separate plot, the waveform at the current index in the RCG and the corresponding footprint in the plot of a map with water mask in background). The tool also allows to plot in dB.

- apply more editing (quality flags ...).
- split our analyses into seasonal climatologies to help detect inaccuracies of the water mask
- introduce the Pulse-Doppler limited footprint so as to discriminate whether the water pixels are at nadir or not (we introduce the WFRN: Fraction of Water Pixels at NADIR).
- repeat the whole analysis for the full Stacks rather than for the RIP only.

In a second development phase we will tackle the following tasks:

- refine the analysis with up to date water masks (Sentinel-1 derived) and use seasonal variants of our own masks to ensure a finely controlled Water Fraction.
- account for roll and pitch angles of the platform when positioning the footprints over the geolocated water mask.
- analyse RCG of the Individual Echoes (L1A products) in conjunction with masks.
- correct tracker range for tropospheric path delays to accurately compute the footprints.
- analyse how the outcome of this work could impact retracers and ease the mapping of water bodies through water detection criteria.
- Perform the same analysis over other areas of interest .

7. BIBLIOGRAPHY

- Fabry, P. and Bercher, N. (2015a). "A step Toward the Automated Production of Water Masks from Sentinel-1 images", Mapping Water Body from Space Conference, 18-19 March 2015. ESRIN, Frascati. [Oral communication](#).
- Fabry, P. and Bercher, N. (2015b). "Characterization of SAR Mode Altimetry over Inland Water". In Proceedings of the Sentinel-3 for Science Workshop, 2-6 June, Venice, Italy. Oral communication and paper. [Download from chronos.altihydrolab.fr](#).
- Fabry P., Bercher N. (2015c). « New Characterization of SAR Mode Altimetry Data over Inland Waters », Keynote talk. In proceedings of the HydroSpace_2015 Workshop (not yet published). September 15-17, ESRIN, Frascati, Italy.
- ESA-UCL, CryoSat-2 Product Handbook, April 2013. <http://wiki.services.eoportal.org/tiki-index.php?page=Cryosat+Documents>
- NGA-USGS, SRTM Water Body Data Product Specific Guidance (v.2.0, March 12, 2003), http://dds.cr.usgs.gov/srtm/version2_1/SWBD/SWBD_Documentation/, NASA/NGA.